

EFFECT OF DIELECTRIC CONFINEMENT ON OPTICAL PROPERTIES OF COLLOIDAL NANOSTRUCTURES

A. V. Rodina^{a*}, *Al. L. Efros*^{b**}

^a *Ioffe Institute*
194021, Saint-Petersburg, Russia

^b *Naval Research Laboratory, DC 20375, Washington, USA*

Received November 17, 2015

We review the effects caused by a large difference in the dielectric constants of a semiconductor and its surrounding in colloidal semiconductor nanostructures (NSs) with various shapes, e.g., nanocrystals, nanorods, and nanoplatelets. The difference increases the electron–hole interaction and consequently the exciton binding energy and its oscillator transition strength. On the other hand, this difference reduces the electric field of a photon penetrating the NS (the phenomenon is called the local field effect) and reduces the photon coupling to an exciton. We show that the polarization properties of the individual colloidal NSs as well as of their randomly oriented ensemble are determined both by the anisotropy of the local field effect and by the symmetry of the exciton states participating in optical transitions. The calculations explain the temperature and time dependences of the degree of linear polarization measured in an ensemble of CdSe nanocrystals.

Contribution for the JETP special issue in honor of L. V. Keldysh's 85th birthday

DOI: 10.7868/S0044451016030159

1. INTRODUCTION

In low-dimensional semiconducting structures, the free motion of electrons and holes is limited by their spatial confinement. In quantum wells, which are referred to as 2D structures in what follows, their motion is limited in one dimension. In quantum wires, to be referred to as 1D structures, their motion is limited in two dimensions, and, finally, in quantum dots and nanocrystals, which are sometimes called 0D structures, their motion is limited in all three dimensions. These confinements generally increase the energy of electron–hole Coulomb interactions and modify (most commonly, increase) the oscillator transition strength of the band-edge optical transitions. In addition to the spatial confinement of free-carrier motion, the low-dimensional semiconductor structures are characterized by a difference in the dielectric constants inside the structures, ϵ^{in} , and in the surrounding media, ϵ^{out} . Such a difference leads to an additional dielectric confinement and affects the electron–hole Coulomb

interaction. The dielectric confinement effect is usually very small in semiconductor/semiconductor heterostructures due to very close values of the dielectric constants, i.e., when the ratio or dielectric contrast is $k = \epsilon^{in}/\epsilon^{out} \approx 1$. In 1979, Keldysh [1] demonstrated that the dielectric confinement strongly affects excitons in the semiconductor/dielectric structures. Several dielectric confinement effects were discussed for semiconductor/dielectric and semiconductor/vacuum structures [1–6], where the contrast k can be as large as 12. It turns out that dielectric confinement becomes even more significant in nanosize anisotropic structures such as porous Si [7, 8], nanowires [9, 10], and various colloids, e.g., nanorods [11–13] and nanoplatelets [14, 15], because it strongly affects the energy spectra of excitons, their selection rules, and their optical polarization properties.

In thin semiconducting films, the electric field of the carriers penetrates into the surrounding media with a small dielectric constant, resulting in a considerable increase in their interaction [1, 2]. This phenomenon leads to the following important consequences [5]: (i) an enhancement of the exciton binding energy and (ii) a decrease in the exciton effective radius a_{ex} . This decrease in turn increases the exciton os-

* E-mail: anna.rodina@mail.ioffe.ru

** E-mail: efros@nrl.navy.mil

cillator strength and the electron–hole short-range exchange interaction, the two characteristics that control the band-edge optical properties of the film. This idea opens a way to control the optical properties of nanostructures via varying the contrast of the dielectric constants [5].

In considering the dielectric confinement effect, however, one has to take into account the renormalization of the electric field of the light that penetrates into the nanostructure (NS) and interacts with the excitons. Such a renormalization, known as the local field effect [16, 17], (i) decreases the probability of the exciton radiative transitions and (ii) leads to a dependence of absorption and photoluminescence on the direction of the electric field of light [4, 6]. The light–matter interaction strength also depends on the angle between the electric field vector and the NS long and short axes [18].

In individual colloidal NSs, the polarization of photoluminescence is determined not only by the anisotropy of the local field effect [6, 19, 20] but also by the exciton fine structure and the selection rules for exciton optical transitions [21–23]. In an ensemble of colloidal NSs, individual crystals are usually randomly oriented. At first glance, this should lead to the absence of any polarization properties. But this is not the case in reality. Due to the local field effect, linearly polarized light selectively excites those NSs whose largest dimension is parallel to the vector polarization of light. The light subsequently emitted by the same NSs is also predominantly polarized along the same direction. This leads to a strong polarization memory effect [7, 24], which for colloidal NSs also depends on the anisotropy of the selection rules for the exciton optical transition [24], and to the nonlinear effects such as the optically induced polarization anisotropy [8, 25].

In this review, we discuss the effect of dielectric confinement on polarization properties and radiative decay of variously shaped nanoscale semiconductor structures. We first discuss the effect of dielectric confinement on the exciton binding energy and the oscillator transition strength in different semiconductor/dielectric NSs. Both the enhancement of the electron–hole Coulomb interaction and the local field corrections are taken into account. We also consider the effect of dielectric confinement on the polarization properties of photoluminescence and selective excitation in individual colloidal NSs with different shapes such as nanocrystals, nanorods, and nanoplatelets, and show how these phenomena lead to the polarization memory effect observed in ensembles of randomly oriented NSs.

2. DIELECTRIC CONFINEMENT AND ENHANCEMENT OF COULOMB INTERACTION

Following the first theoretical predictions [1–5], the modification of the Coulomb interaction between charge carriers by the dielectric confinement of semiconducting NSs embedded in media with small dielectric constants was further studied experimentally and theoretically in quantum wires [9, 10], thin films, near-surface quantum wells [26, 27], superlattices [28], and quantum dots [29–33].

Generally, the dielectric confinement not only modifies the Coulomb interaction between charges, but also affects the energy of a single particle, electron or hole, localized inside the NS. This effect can be described as the effective interaction of the electron (hole) with its own image charge that is positioned outside of the NSs [34, 35]. The respective electron (hole) self-energy potential $V_{self}(\mathbf{r}_{e(h)})$ should be added to the spatial confining potential $V_{pot}(\mathbf{r}_{e(h)})$ created by the potential profile of the NS. The resulting confining potential can be written as

$$V_{conf}(\mathbf{r}_{e(h)}) = V_{pot}(\mathbf{r}_{e(h)}) + V_{self}(\mathbf{r}_{e(h)}). \quad (1)$$

The self-energy potential $V_{self}(\mathbf{r})$ is always proportional to $\epsilon^{in} - \epsilon^{out}$ [34]. It is repulsive in semiconducting NSs, where $k = \epsilon^{in}/\epsilon^{out} > 1$, and describes an effective surface polarization field pulling the carriers into the NS. This repulsive potential in NSs of any shape leads to an additional confinement of the carriers [10–12, 14, 26–33, 36–39].

The effective Coulomb interaction between an electron and a hole, accounting for the dielectric confinement, becomes

$$V_{Coul}(\mathbf{r}_e, \mathbf{r}_h) = -\frac{e^2}{\epsilon^{in}|\mathbf{r}_e - \mathbf{r}_h|} - V_{im}(\mathbf{r}_e, \mathbf{r}_h). \quad (2)$$

Here, the second term describes the interaction of one charge with the surface polarization charge created by the other charge, which can be effectively written as the interaction with the image charge.

Specific expressions for the potentials $V_{self}(\mathbf{r}_{e(h)})$ and $V_{im}(\mathbf{r}_e, \mathbf{r}_h)$ depend on the NS shape and geometry. In the case of strong three-dimensional confinement, the notion of an exciton as a mobile excitation should be used with some care [5]. Indeed, if the radius a

of the quantum dot is smaller than the effective exciton radius $a_B = \epsilon^{in} \hbar^2 / (e^2 \mu)$ in the bulk semiconductor (here $\mu = (m_e + m_h) / m_e m_h$ is the exciton reduced mass), the Coulomb energy $\propto (a_B/a)$ can be considered a small correction to the electron and hole quantum-size energy levels $\propto (a_B/a)^2$. However, the dielectric confinement corrections should be taken into account even for spherical quantum dots, especially for colloidal nanocrystals (NCs) synthesized in a glass matrix or in solution [29–33, 36–39].

In spherical NCs, the self-corrections $V_{self}(\mathbf{r}_e) + V_{self}(\mathbf{r}_h)$ nearly cancel the additional interchange correction from $V_{im}(\mathbf{r}_e, \mathbf{r}_h)$ due to the local neutrality, which the NC keeps even after the excitation of an electron–hole pair. Therefore, taking the dielectric confinement into account does not lead to any modification of the optical transition energies. The cancelation is exact for the ground-state transition in the case of simple parabolic conduction and valence bands when the wave functions of electrons and holes in the strong quantization regime are identical. The cancelation is partially lifted when the complex structure of the valence band is taken into account [32]. However, even in this strong confinement regime, the surface polarization energy described by $V_{self}(\mathbf{r}_{e(h)})$ can be detected as the charging energy in tunneling experiments [37–39]. When the correlation of the electron and hole motions due to their Coulomb interaction is taken into account, the dielectric confinement effect causes a small increase in the exciton binding energy and exciton oscillator strength [31–33]. A larger effect can be expected in the weak confinement regime, when the NC radius a is larger than a_B .

Importantly, in 1D and 2D structures, spatial confinement already leads to an increase in the exciton binding energy and a decrease in the exciton effective length in the free motion direction. This consequently increases the exciton oscillator transition strength [5]. The effect of dielectric confinement in 1D or 2D nanostructures further enhances these phenomena because a large share of the electromagnetic field penetrates into the surrounding medium, which has a small dielectric constant. Analytic estimations for these effects for infinite quantum wires and quantum wells in different regimes were summarized by Keldysh [5]. Later on, more elaborate theoretical calculations for realistic quantum wires demonstrated good agreement with experimental results for the GaAs, CdSe, and InP quantum wires with a diameter $d \sim 4\text{--}6$ nm crystallized in a dielectric matrix [28]. It was shown that the dielectric contrast $k = \epsilon^{in} / \epsilon^{out} > 1$ leads to a considerable enhancement of the exciton binding energies by a fac-

tor of k^2 . The experimental binding energy increase ranges from 120 meV to 260 meV. The corresponding decrease in the exciton effective length $a_{ex} \propto a_B/k$ results in an increase of the exciton oscillator strength, $f_{ex} \propto a_B^3 / (d^2 a_{ex}) \propto k$.

The effects of the dielectric confinement on potentials $V_{self}(\mathbf{r}_{e(h)})$ and $V_{im}(\mathbf{r}_e, \mathbf{r}_h)$ in NSs that have the shape of an elongated ellipsoid of revolution described as $(x^2 + y^2)/b^2 + z^2/c^2 = 1$ with $c/b > 1$ have been considered for chemically synthesized CdSe [11] and PbSe colloidal nanorods [12]. It was found that the dielectric contrast $k = \epsilon^{in} / \epsilon^{out} > 1$ considerably increases the energy of the electron and hole quantum-size levels and significantly enhances the exciton binding energies [11, 12]. In the case of the PbSe nanorods and nanowires, however, the increase in the binding energy is almost exactly compensated by the electron and hole self-interaction terms, similarly to the situation in spherical NCs [12]. The effect of the dielectric contrast on the exciton effective length in PbSe nanorods and nanowires was also found to be small. Hence, the linear optical spectra of PbSe nanowires and nanorods are not sensitive to the dielectric constant of the surrounding medium. The cancelation of the Coulomb energies in the ground exciton of PbSe was attributed to a similar charge compensation. The mirror symmetry of the conduction and valence bands in PbSe makes the wave functions of the electron and hole transverse motion nearly identical. The close values of effective masses along the long axes also make the electron and hole contributions to the 1D exciton wave function identical. In contrast, the modification of the exciton optical transitions in the CdSe nanorods due to the dielectric contrast was shown to be significant [11].

For 2D quantum wells or thin films surrounded by a dielectric medium with constants $\epsilon_{(1)}^{out}$ and $\epsilon_{(2)}^{out}$ on two sides of the layer, the effect of the dielectric contrast $k = 2\epsilon^{in} / (\epsilon_{(1)}^{out} + \epsilon_{(2)}^{out})$ on the 2D excitons depends on the ratio between the well thickness d and a_B . As was discussed by Keldysh [5], the effects are most pronounced for extremely thin films, as defined by the inequality $d < a_B/k^2$. In this case, the exciton problem becomes essentially a two-dimensional Coulomb problem with the effective dielectric constant $\epsilon^{out} = (\epsilon_{(1)}^{out} + \epsilon_{(2)}^{out})/2$. The exciton binding energy is then again increased by the factor k^2 with respect to the bulk exciton binding energy and the exciton effective length decreases as $a_{ex} \propto a_B/k$. This would correspond to an increase in the exciton oscillator strength as $f_{ex} \propto a_B^3 / (d a_{ex}^2) \propto k^2$. But for conventional quantum wells and thin layers, the condition of an extremely thin film can hardly be realized, partly due to effects

of the electron energy spectrum nonparabolicity [5]. In fact, with the increase in the electron energy E_e due to the spatial confinement in the direction perpendicular to the well plane, the electron effective mass and hence the exciton reduced mass $\mu(E_e)$ increase. As a result, the exciton Bohr radius $a_B(E_e)$ calculated with the increased $\mu(E_e)$ decreases and $a_B(E_e)/k^2 < d < a_B/k^2$ corresponds to the regime of a moderately thin film. In this case, the exciton binding energy increases as $\log k^2$, while the exciton effective length remains unaffected by the dielectric contrast [5].

As shown theoretically and experimentally, the dielectric enhancement of the exciton binding energy can be more easily achieved in near-surface quantum wells [26, 27]. In these structures, it suffices to consider only one interface, with the dielectric contrast existing between the well material and the vacuum. In InGaAs/GaAs heterostructures with the well thickness $d = 5$ nm and different cap layer thicknesses separating the well from the vacuum, the strong dielectric enhancement of the exciton binding energy due to the dielectric contrast $k = 12$ was calculated and measured directly via the increase in the splitting between the $2s$ and the $1s$ exciton states as the cap layer thickness decreases. In addition, the decrease in the diamagnetic shift coefficient $\propto a_{ex}^2$ was calculated and measured as evidence of the dielectric reduction in the exciton effective length.

Recently, a new type of atomically flat noncrystalline colloids, known as nanoplatelets or colloidal quantum wells, was introduced [40]. Due to their atomic flatness and strictly quantized thickness distribution, they are ideal objects to test the effects of the dielectric contrast predicted for extremely thin films. Theoretical calculations conducted within the multiband $\mathbf{k} \cdot \mathbf{p}$ model [15], the tight-binding model [14], and the *ab initio* approach [41] all demonstrated the importance of the dielectric contrast for the enhancement of the electron and hole confinement energies through self-interaction with their own image charges as well as for the huge increase in the exciton binding energy. For the exciton ground state, the attractive effect of the electron and hole image charges partly compensates the dominant repulsive effect of single-particle self-energies. For the excited states nS , the electron–hole interaction decreases and the effect of self-energies prevails more and more as n increases, such that the nS transitions are strongly blueshifted with respect to the bare single-particle gap [14]. It has been suggested that the huge predicted values of exciton binding energies could be tested experimentally by comparing one-photon and

two-photon absorption spectra, giving access to respective S and P exciton states. The decrease in the exciton effective radius a_{ex} in the lateral direction due to the dielectric contrast was also predicted theoretically [15] and most probably found experimentally by evaluating the splitting between the bright and dark ground-state excitons [42]. This splitting was found to be an order of magnitude larger than the typical one in II–VI epitaxial quantum wells of similar thickness. This large difference can be regarded as evidence for the enhanced electron–hole exchange interaction $\propto (a_B)^3/da_{ex}^2$ due to dielectric confinement.

At the end of this section, we briefly mention some important questions concerning the values of the dielectric constants that determine the dielectric contrast in colloidal structures. There is uncertainty about the dielectric constant of the surrounding medium, ϵ^{out} , because colloidal NSs can be terminated by different organic ligands and placed in different solvents. At the same time, this provides the possibility of directly testing the effect of different ϵ^{out} on the optical properties of otherwise identical colloidal NSs.

Even more complicated problems arise when we discuss the dielectric constant ϵ^{in} inside the NS and its size dependence [43]. General arguments as well as numerical tight-binding calculations showed that irrespective of the size, one locally recovers the bulk dielectric function for the macroscopic component of the field except in a thin surface layer of the order of a few Fermi wavelengths [44]. It was suggested that the dependence of ϵ^{in} on the NS size could be reproduced directly from the use of the bulk response function [44]. But even in bulk semiconductors, some uncertainty remains as to which values of ϵ^{in} should be used for the screening of the Coulomb interaction [45]: the static (low-frequency) dielectric constant $\epsilon^{in}(0)$ or the high-frequency dielectric constant $\epsilon^{in}(\infty)$. In polar bulk semiconductors, the screening of the Coulomb interaction in the exciton depends on the distance between the electron and the hole. In the case of a simple parabolic band, this dependence can be described by the models proposed by Haken [46] or by Pollmann and Büttner [47]. Both models predict that at distances r much longer than the characteristic electron–polaron and hole–polaron radii $l_{e,h} = \sqrt{\hbar^2/2m_{e,h}E_{LO}}$, where E_{LO} is the optical phonon energy, the Coulomb interaction is screened by $\epsilon^{in}(0)$, while at $r \ll l_{e,h}$, the value of $\epsilon^{in}(\infty)$ should be used. The Haken model, however, is more suitable for the excitons with $a_{ex} < l_{e,h}$ and is therefore sometimes used to describe size-dependent Coulomb screening in NSs [39, 45]. However, for small-size NSs, the condition

$r \ll l_{e,h}$ is a reasonable approximation and the value of $\epsilon^{in}(\infty)$ has been used for all the effects of dielectric enhancement of excitons considered above.

3. LOCAL FIELD EFFECT AND ITS ANISOTROPY

The large contrast $k = \epsilon^{in}/\epsilon^{out}$ of dielectric constants inside and outside the NS leads to a renormalization of the electric field \mathbf{E}^{in} inside the NS with respect to the homogeneous external field \mathbf{E}^{out} in the surrounding medium [18]. In an irregularly shaped NS, the field can be highly nonuniform and, in the most general case, there is no simple analytic form to describe the distribution of the field inside the NS. However, for some simple geometrical shapes, such as infinite 1D nanowires, 2D quantum wells, ellipsoids or spheres, the field inside the NS is uniform and proportional to the field outside. For the ellipsoid of revolution, the projection of the electric field inside E_α^{in} and outside E_α^{out} the NC are related as

$$E_\alpha^{in} = \frac{E_\alpha^{out}}{1 + n^{(\alpha)}(k - 1)}, \quad (3)$$

where $\alpha \equiv x, y, z$, the depolarization factors $n^{(\alpha)}$ depend only on the shape of the ellipsoidal NC and do not depend on its volume V , and $n^{(z)} + n^{(x)} + n^{(y)} = 1$. For a sphere of radius a , the depolarization factors are $n^{(z)} = n^{(x)} = n^{(y)} = 1/3$.

If the NC shape is described as $(x^2 + y^2)/b^2 + z^2/c^2 = 1$, the depolarization factors depend only on the aspect ratio b/c [18]:

$$n^{(z)} = \frac{1 - e^2}{2e^3} \left(\ln \frac{1 + e}{1 - e} - 2e \right) \leq \frac{1}{3} \quad \text{if } 0 < b/c \leq 1, \quad 0 \leq e < 1, \quad (4)$$

$$n^{(z)} = \frac{1 + e^2}{e^3} (e - \arctan e) \geq \frac{1}{3} \quad \text{if } 0 < c/b \leq 1, \quad 0 \leq e < \infty, \quad (5)$$

$$n^{(x)} = n^{(y)} = [1 - n^{(z)}]/2, \quad e = \sqrt{|1 - b^2/c^2|}. \quad (6)$$

The case $b/c < 1$ describes prolate ellipsoids elongated along the z direction, while $b/c > 1$ corresponds to oblate structures. For small deviations of the spherical shape $e \ll 1$ and b/c close to unity, we obtain

$$n^{(z)} \approx \frac{1}{3} \mp \frac{2}{15}e^2 = \frac{1}{5} + \frac{2}{15} \left(\frac{b}{c} \right)^2, \quad (7)$$

$$n^{(x)} = n^{(y)} \approx \frac{1}{3} \pm \frac{1}{15}e^2 = \frac{2}{5} - \frac{1}{15} \left(\frac{b}{c} \right)^2. \quad (8)$$

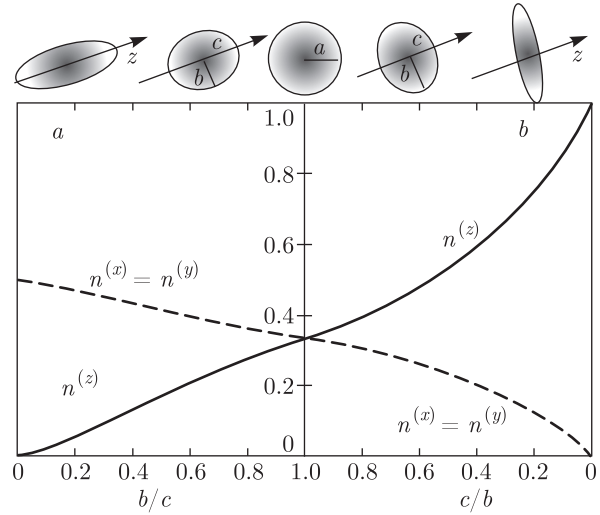


Fig. 1. Dependences of the depolarization factors $n^{(z)}$ (solid lines) and $n^{(x)} = n^{(y)}$ (dashed lines) (a) on the aspect ratio $b/c = a/c$ for prolate NSs and (b) on $c/b = c/a$ for oblate NCs that have the shape of ellipsoids of revolution

In contrast, the limit cases $b/c \ll 1$ and $c/b \ll 1$ describe the 1D structures (nanorods or nanowires) and the 2D case (nearly flat quantum discs or quantum wells). Indeed, in the case $b/c \ll 1$, we obtain from Eq. (4) as $e \rightarrow 1$ that

$$n^{(z)} \approx \left(\frac{b}{c} \right)^2 \left[\ln \left(\frac{2c}{b} \right) - 1 \right] \rightarrow 0, \quad (9)$$

$$n^{(x)} = n^{(y)} \rightarrow \frac{1}{2}.$$

In the case $c/b \ll 1$, we obtain from Eq. (5) as $e \rightarrow \infty$ that

$$n^{(z)} \approx 1 - \frac{\pi c}{2b} \rightarrow 1, \quad n^{(x)} = n^{(y)} \rightarrow 0. \quad (10)$$

These limit values of the depolarization factors can be directly obtained for an infinite 1D cylinder or 2D quantum well [18]. They show that the electric field along the dielectric homogeneous direction, which is directed along the cylinder axis or lies in the plane of the quantum well, is not renormalized, while the electric field perpendicular to the cylinder axis or to the quantum well plane is strongly reduced for the dielectric contrast $k > 1$.

Figure 1 shows the dependences of the depolarization factors $n^{(z)}$ (solid lines) and $n^{(x)} = n^{(y)}$ (dashed lines) on the aspect ratio $b/c = a/c$ for the prolate and $c/b = a/c$ for the oblate ellipsoids of revolution calculated according to respective equations (4) and (5).

When the size of the spatial confinement of the NS is smaller than the wavelength of light, the renormal-

ization of the amplitude of the electric field of light entering the matrix elements for the absorption and spontaneous emission probability is also described by Eq. (3) [17, 48, 49]. In this case, the values of the bulk dielectric constants should be taken at the excitation, ω_a , or detection, ω_d , frequency of the absorbed or emitted light [7], and $k(\omega) = \epsilon^{in}(\omega)/\epsilon^{out}(\omega)$. We note that in this long-wavelength limit, the renormalization of $\epsilon^{in}(\omega)$ in the vicinity of the exciton resonance energy should not be included in the consideration of the local field effect [48].

Because the absorption of light occurs only inside the NS, the probability $W_\alpha^a = W_\alpha(\omega_a)$ to absorb light polarized along the $\alpha = x, y, z$ direction is proportional to $|d_\alpha E_\alpha^{in}|^2$, where d_α is the respective projection of the dipole matrix element of the momentum operator $\hat{\mathbf{p}} = -i\hbar\nabla$ describing the interband optical transition. Therefore, the local field effect reduces W_α^a by the screening factor $D_\alpha^a = 1/[1 + n^{(\alpha)}(k^a - 1)]^2$ with $k^a = k(\omega_a)$. Assuming that at least one of the carriers is well localized inside the NS, as is the case with all colloidal NSs due to very high potential barriers, the probability to emit light $W_\alpha^d = W_\alpha(\omega_d)$ is also reduced by the screening factor $D_\alpha^d = 1/[1 + n^{(\alpha)}(k^d - 1)]^2$ with $k^d = k(\omega_d)$.

In spherical NCs, the screening factors are the same for all polarization directions and are equal to

$$D_x = D_y = D_z = D^{sph} = \left[\frac{3\epsilon^{out}}{2\epsilon^{out} + \epsilon^{in}} \right]^2 = \left[\frac{3}{2+k} \right]^2. \quad (11)$$

As in nonspherical NSs, the depolarization factors for the longer axes are smaller than those for the shorter axes, and the screening factors for the transitions polarized along the longer axes are smaller than those for the shorter axes. In nanowires or nanorods with $b/c \ll 1$, there is no reduction of the transitions polarized along the axis: $D_z = 1$, while the transition probabilities for light polarized perpendicular to the axis are reduced by the local field effect as

$$D_x = D_y = D_\perp^{1D} = \left[\frac{2\epsilon^{out}}{\epsilon^{out} + \epsilon^{in}} \right]^2 = \left[\frac{2}{1+k} \right]^2. \quad (12)$$

In contrast, in quantum wells or disks with $c/b \ll 1$, there is no reduction in the transition probabilities for light polarized in the well plane: $D_x = D_y = 1$, while the transitions polarized perpendicular to the plane are reduced by the local field effect as

$$D_z = D_\parallel^{2D} = \left[\frac{\epsilon^{out}}{\epsilon^{in}} \right]^2 = \left[\frac{1}{k} \right]^2. \quad (13)$$

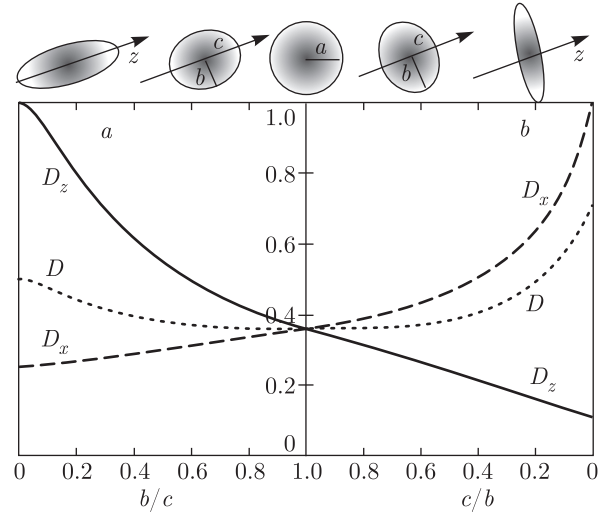


Fig. 2. Dependences of the screening factors D_z (solid lines), $D_x = D_y$ (dashed lines), and $D = (D_x + D_y + D_z)/3$ (dotted lines) (a) on the aspect ratio $b/c = a/c$ for prolate NCs and (b) on $c/b = c/a$ for oblate NCs that have the shape of ellipsoids of revolution, calculated for the dielectric contrast value $k = \epsilon^{in}/\epsilon^{out} = 3$

Figure 2 shows the dependences of the screening factors D_z (solid lines), $D_x = D_y$ (dashed lines), and $D = (D_x + D_y + D_z)/3$ (dotted lines) on the aspect ratio $b/c < 1$ for prolate NSs and on $c/b < 1$ for oblate NSs that have the shape of ellipsoids of revolution calculated for the values of the dielectric contrast $k = \epsilon^{in}/\epsilon^{out} = 3$.

Clearly, the local field effect due to dielectric confinement causes the reduction (screening) of the radiative rate and intensity of the transitions for all polarizations. Neglecting the exciton fine energy structure splitting and assuming the isotropic distribution of the dipole matrix elements $d_x^2 = d_y^2 = d_z^2$ for light absorption at the energy well above the ground-state exciton resonance, the screening effect averaged over all light polarizations is given by the averaged screening factor $D = (D_x + D_y + D_z)/3 = (2D_\perp + D_\parallel)/3$. We can see that the largest reduction of the radiative transition probabilities is expected in spherically symmetric NSs, which are described by the factor $D^{sph} \rightarrow (3/k)^2$ for $k \gg 1$ [17, 48, 49]. For 1D structures, the reduction effect is described by the factor $(2D_\perp^{1D} + 1)/3 \rightarrow 1/3$ for $k \gg 1$. In 2D structures, the reduction effect is described by the factor $(2 + D_\parallel^{2D})/3 \rightarrow 2/3$ for $k \gg 1$. This is the smallest reduction because the electric field of light polarized in the QW plane is not affected. This suppression of the radiative probability in thin 2D NSs, e.g., in colloidal nanoplatelets, is overpowered by the

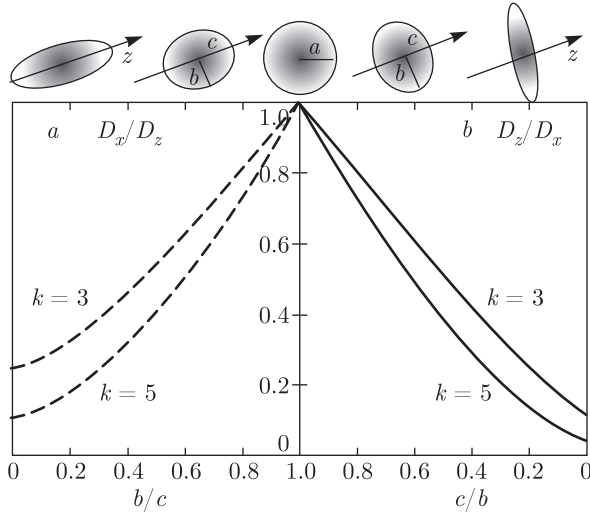


Fig. 3. Dependence of the screening factors ratio (a) $1/R = D_x/D_z$ (dashed lines) and (b) $R = D_z/D_x$ (solid lines) on (a) the aspect ratio $b/c = a/c$ for prolate and (b) on $c/b = c/a$ for oblate NCs that have the shape of ellipsoids of revolution, calculated for two dielectric contrast values $k = \epsilon^{in}/\epsilon^{out} = 3$ and $k = 5$

enhancement of the exciton oscillator strength $\propto k^2$ due to the dielectric confinement discussed above.

Figure 3 shows the dependences of the screening factor ratio $R = D_z/D_x$ and its inverse $1/R$ on the aspect ratio $b/c < 1$ for prolate and on $c/b < 1$ for oblate nanocrystals whose shape is described by ellipsoids of revolution. Calculations are conducted for two values of the dielectric contrast $k = \epsilon^{in}/\epsilon^{out} = 3$ and $k = 5$.

4. POLARIZATION PROPERTIES OF THE EXCITON ABSORPTION AND EMISSION IN NANOSTRUCTURES

In spherically symmetric structures, the polarization properties of the exciton absorption and emission are determined solely by the dipole matrix elements d_α ($\alpha = x, y, z$) and the exciton energy fine structure. In this case, the local field effect due to the dielectric confinement causes only the reduction of the radiative rate $1/\tau_r$ and probabilities $W_\alpha^{a(d)} \propto D_\alpha^{a(d)}$ of the optical transitions for all polarizations α by the factor D^{sph} [17, 48–50]. Calculations of the decay times and photoexcitation probabilities also require some estimation of the effective refractive index of the matrix where the NCs are embedded. In the case where the total volume of the NCs is much smaller than the volume of the dielectric matrix outside, it can be estimated as $\sqrt{\epsilon^{out}}$ [49, 50].

In nonspherical NSs, the local field effect becomes anisotropic and directly affects the polarization properties of the exciton optical transitions. In the case of an isotropic distribution of the dipole matrix elements $d_x^2 = d_y^2 = d_z^2 = d^2$, the polarization of the optical transitions depends only on the anisotropy of D_α . With this assumption, the polarization of the absorption of light propagating perpendicular to the wire

$$\rho = \frac{I_{\parallel} - I_{\perp}}{I_{\parallel} + I_{\perp}}, \quad (14)$$

where I_{\parallel} and I_{\perp} are the intensities of the light polarized parallel and perpendicular to the wire long axis, was first predicted [6] and then observed and described [19, 20] for the InGaAs/InP quantum-well wire structures. In this case, the polarization is given by

$$\rho \approx \sigma = \frac{\langle E_{\parallel} \rangle^2 - \langle E_{\perp} \rangle^2}{\langle E_{\parallel} \rangle^2 + \langle E_{\perp} \rangle^2} = \frac{D_{\parallel} - D_{\perp}}{D_{\parallel} + D_{\perp}} = \frac{R - 1}{R + 1}. \quad (15)$$

Clearly, the increase and saturation of the polarization with an increase of wire length/wire width ratio [19, 20] is related to the dependence of the ratio $1/R = D_x/D_z$ on the aspect ratio b/c shown in Fig. 3a. The ultimate case of the 1D infinite NS studied for the semiconductor/dielectric quantum wires [10, 51] and for the isolated InP nanowires [52] is given by $\sigma^{1D} = (1 - D_{\perp}^{1D})/(1 + D_{\perp}^{1D})$.

It is worth noting that in the case of a planar 2D NS, one cannot observe the polarization of light at normal incidence. Generally, for an ellipsoidal-shape NS, the probability for the optical transition with a light polarization vector \mathbf{e} is given by [7, 8, 53]

$$P_{\mathbf{e}} = D_{\perp} + (D_{\parallel} - D_{\perp})(\mathbf{c} \cdot \mathbf{e})^2 = D_{\perp} + (D_{\parallel} - D_{\perp}) \cos^2 \Theta_{\mathbf{e}}, \quad (16)$$

where the \mathbf{c} axis of the NC is directed along the z direction and $\Theta_{\mathbf{e}}$ is the angle between \mathbf{e} and \mathbf{c} (see the light geometry sketch in Fig. 4a).

For light propagating at an angle Θ to the \mathbf{c} axis, $\cos^2 \Theta_{\mathbf{e}} = \sin^2 \Theta \cos^2 \Phi$. The probability of the optical transition created by unpolarized light propagating at an angle Θ to the \mathbf{c} axis can be obtained as

$$P_{\mathbf{k}} = \frac{1}{2\pi} \int_0^{2\pi} P_{\mathbf{e}} d\Phi = 0.5(D_{\parallel} + D_{\perp})[1 - \sigma(\mathbf{c} \cdot \mathbf{k})^2] = 0.5(D_{\parallel} + D_{\perp})[1 - \sigma \cos^2 \Theta], \quad (17)$$

where \mathbf{k} is the light wave vector.

Polar plots of the angular dependence of the transition probability $P_{\mathbf{e}}$ on the angle $\Theta_{\mathbf{e}}$ between polarization vector \mathbf{e} and the c axis direction, and of $P_{\mathbf{k}}$ on

the angle Θ between wave vector \mathbf{k} and the c axis direction, are shown in Fig. 4b and c. Calculations are conducted for ellipsoids with various aspect ratios b/c assuming that the dipole projections are equal to each other, $|d_x|^2 = |d_y|^2 = |d_z|^2$. We note that the absolute values of the probability (distance from the origin) are not scaled and reflect different local field reduction factors D for different aspect ratios, such that the total integrated probability is proportional to D . The full range of angles up to 360 degree is shown for better visualization.

The polarization of light absorbed or emitted by an individual NS can now be found as

$$\rho(\Theta, \Phi) = \frac{I_{\parallel} - I_{\perp}}{I_{\parallel} + I_{\perp}} = \frac{(R - 1) \sin^2 \Theta \cos 2\Phi}{(1 + \cos^2 \Theta) + R \sin^2 \Theta}, \quad (18)$$

where the anisotropy parameter $R = D_{\parallel}/D_{\perp}$ depends on the aspect ratio b/c and the dielectric contrast k as discussed in the preceding section. Equation (18) is a generalization of Eq. (15) to the case of an arbitrary geometry of light propagation. The polarization is maximal when the analyzer parallel axis \mathbf{e} is set such that $\cos 2\Phi = 1$. Figure 4d shows the angular dependence of the linear polarization degree $\rho_{\mathbf{k}} \equiv \rho(\Theta, 0^\circ)$ on the angle Θ between the wave vector \mathbf{k} and the c axis direction. In the limit cases of the infinite 1D quantum wire and 2D quantum well structures ($b/c = 0$ and $c/b = 0$), we obtain

$$\rho_{\mathbf{k}}^{1D} = \frac{[(1+k)^2 - 4] \sin^2 \Theta}{4(1 + \cos^2 \Theta) + (1+k)^2 \sin^2 \Theta}, \quad (19)$$

$$\rho_{\mathbf{k}}^{2D} = \frac{(1 - k^2) \sin^2 \Theta}{k^2(1 + \cos^2 \Theta) + \sin^2 \Theta}. \quad (20)$$

The above analysis of the polarization properties of the emitted and absorbed light was done under the assumption of isotropic exciton dipole selection rules: $d_x^2 = d_y^2 = d_{\perp}^2 = d_z^2 = d_{\parallel}^2$. In most cases, however, to describe the polarization properties of single or ensemble semiconductor NSs, we have to take the exciton fine energy structure into account. The symmetry of the lowest exciton states and the selection rules for their optical transitions depend strongly on the size and shape of the NS as well as on the internal symmetry of the crystal lattice. The exciton states are formed with the holes from the heavy-hole and light-hole manifolds having different selection rules and are affected by the electron-hole exchange interaction enhanced by the spatial confinement.

In this case, the effective dipole matrix elements of emitted light have to be calculated taking into account all the emitting exciton states and their populations,

controlled by thermal distribution [11, 54]. This phenomenon can be easily incorporated in the previous consideration by replacing D_{\parallel}^d and D_{\perp}^d with $D_{\parallel}^d |d_{\parallel}^d|^2$ and $D_{\perp}^d |d_{\perp}^d|^2$ in all expressions above, where

$$|d_{\parallel}^d|^2 = \sum_i N_i |d_{\parallel}^i|^2, \quad (21)$$

$$|d_{\perp}^d|^2 = \sum_i N_i |d_{\perp}^i|^2. \quad (22)$$

Here N_i is the relative population of the i th exciton state ($\sum_i N_i = 1$), and $|d_{\parallel}^i|^2 = |d_z^i|^2$ and $|d_{\perp}^i|^2 = |d_x^i|^2 = |d_y^i|^2$ describe the squares of the dipole matrix elements of $\hat{\mathbf{p}}_z$ and $\hat{\mathbf{p}}_{x,y}$ for the i th exciton state. This substitution results in generalized expressions for the linear polarization degree of the light emitted by an individual NS. To generalize Eq. (18), we must replace the local field anisotropy factor R in this expression by the total anisotropy parameter $r_d = R f_d$, where the factor $f_d = |d_{\parallel}^d|^2 / |d_{\perp}^d|^2$ describes the anisotropy of the selection rules for the exciton-emitting states.

For example, if the exchange interaction and heavy-hole-light-hole mixing are neglected, the dipole matrix elements of the heavy-hole and light-hole excitons are [54]

$$|d_{\parallel}^{hh}|^2 = 0, \quad |d_{\perp}^{hh}|^2 = \frac{P^2}{2}, \quad (23)$$

$$|d_{\parallel}^{lh}|^2 = \frac{2P^2}{3}, \quad |d_{\perp}^{lh}|^2 = \frac{P^2}{6}, \quad (24)$$

where P is the Kane matrix element of the band-to-band transitions in zinc-blende or wurtzite semiconductors in the quasicubic approximation. Therefore, the selection rule anisotropy can be respectively described by $f_d^{hh} = 0$ and $f_d^{lh} = 4$ for the heavy-hole and light-hole excitons. Accounting for the different admixtures of the light-hole and heavy-hole exciton states in different exciton states in weak and strong quantization regimes in zinc-blend and wurtzite nanowires [54] allows describing the polarization properties and temperature-induced polarization reversal observed in single GaAs nanowires [54, 55].

For colloidal NCs, nanowires and nanorods, the short-range interaction enhanced by confinement should also be taken into account. As a result, the bright (dipole-allowed) exciton states are characterized by the momentum projection F on the c -axis [11, 23]. The splitting between the states strongly depends on the nanowire or nanocrystal radius and the b/c aspect ratio [11, 23, 56]. In the case of a small b/c ratio, the optical properties of the CdSe colloidal nanorods are determined by the lowest bright exciton states

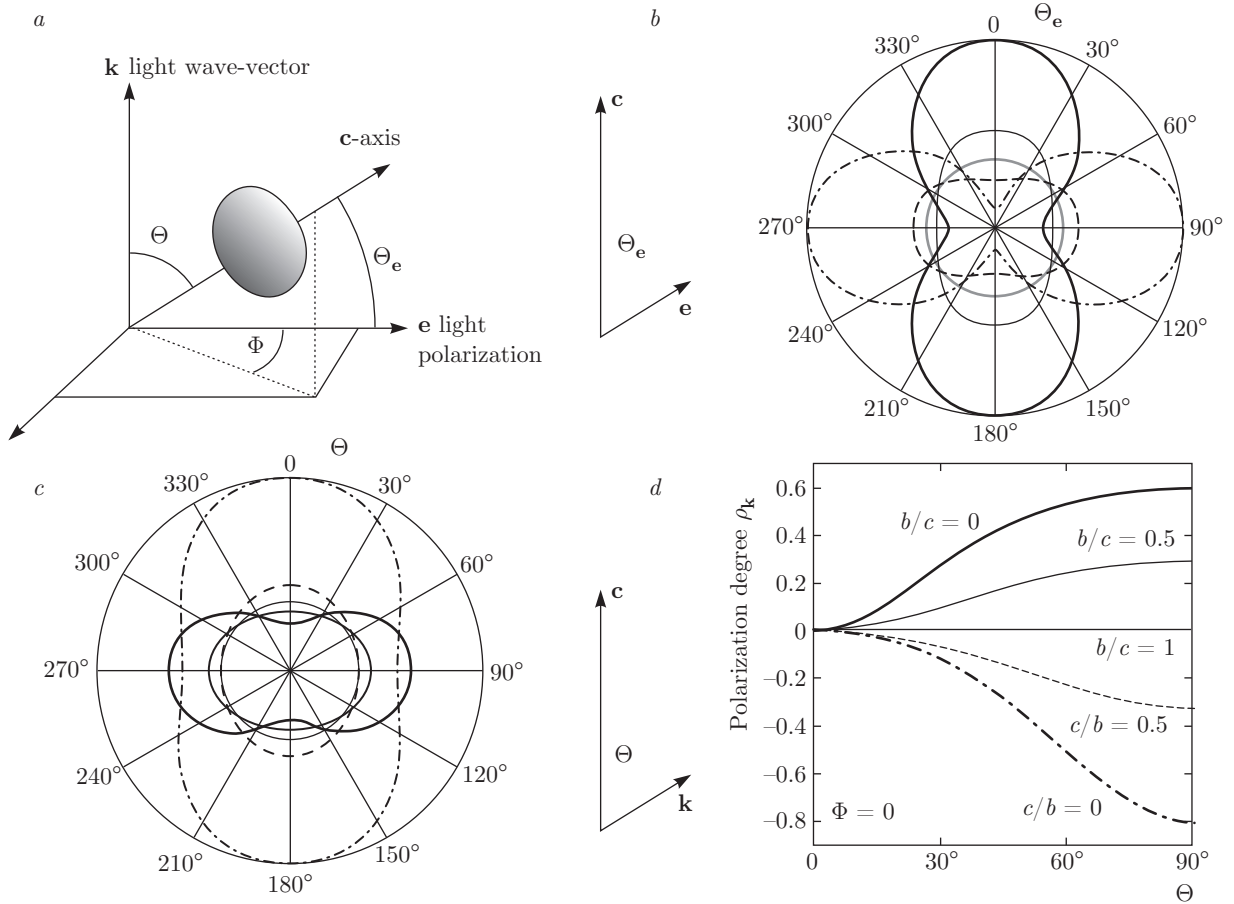


Fig. 4. (a) Geometry of light propagation; (b) dependence of the optical transition probability $P_e(\Theta_e)$ on the angle Θ_e between the polarization vector of light e and the c -axis of the NC (polar plot); (c) dependence of the optical transition probability $P_k(\Theta)$ on the angle Θ between the wave vector k of light and the c -axis of the NC (polar plot); (d) angular dependence of the linear polarization degree $\rho_k(\Theta) = \rho(\Theta, \Phi = 0)$ on the angle Θ between the wave vector k of the light and the c -axis of the NC. Calculations are conducted for ellipsoidal-shape NSs with isotropic dipoles ($|d_x|^2 = |d_y|^2 = |d_z|^2$) and the dielectric contrast $k = 3$. The dependences shown by thick solid lines were calculated for $b/c = 0$, by thin solid lines for $b/c = 0.5$, by grey lines for $b/c = 1$, by dashed lines for $c/b = 0.5$, and by dot-dashed lines for $c/b = 0$. In (b) and (c), the range of angles up to 360° is shown for better visualization. The absolute values of probability in (b) and (c) range from 0 (origin) to 1

with the projection $F = \pm 1$ and $F = 0$, which are formed mostly from the light-hole manifold. The dipole matrix elements of the momentum operator $\hat{p}_{\pm 1} = (\hat{p}_x \pm i\hat{p}_y)/2$ calculated for $F = \pm 1$ excitons are expressed via the nondegenerate dipole of the $F = 0$ exciton d_0 : $|d_{+1}|^2 = |d_{-1}|^2 = |d_0|^2/8$. This leads to a dependence of the parameter $f_d(T)$ and consequently $r_d(T) = Rf_d(T)$ on the temperature T as [11]

$$r_d(T) = R \frac{|d_{\parallel}^d|^2}{|d_{\perp}^d|^2} = R \frac{N_0 |d_0|^2}{N_{+1} |d_{+1}|^2 + N_{-1} |d_{-1}|^2} = 4R \exp \frac{E_{\pm 1} - E_0}{k_B T}, \quad (25)$$

where $E_{\pm 1} < E_{\pm 0}$ are the respectively energies of the exciton states with $F = \pm 1$ and $F = 0$, and k_B is the Boltzmann constant. Replacing R in Eq. (18) by r_d from Eq. (25) allows us to describe the temperature dependence of the linear polarization degree of light emitted by a single CdSe nanorod. This theory, without any fitting parameters, provides an excellent agreement with experimental data and explains the high 87% degree of linear polarization along the long axis observed at room temperature for $\Theta = 90^\circ$ [11, 57]. At low temperatures, however, the degree of PL polarization should drop significantly due to the depopulation of the $F = 0$ exciton state, providing linearly polarized luminescence [11]. This is directly reflected in the ex-

ponential decrease of the anisotropy parameter f_d and hence r_d in Eq. (25) as the temperature decreases.

The absence of local field screening for photons emitted by the $F = 0$ exciton state contributes also to the faster radiative decay in CdSe nanorods: for sufficiently elongated NRs at room temperature, the radiative lifetime is as short as 500 ps compared to ≈ 20 ns measured in CdSe NCs [58]. The strong dependence of the radiative lifetimes and polarization properties of the CdSe nanorods on the b/c aspect ratio was also reported in [56].

To describe the polarization properties for nonresonant absorption of light by a single colloidal NS, the model of isotropic excitons and Eq. (18) can typically be used. This was demonstrated by directly measuring the absorption anisotropy in colloidal CdSe quantum rods [13]. However, to explain the wavelength-dependent polarization measured at the resonant absorption of ensembles of CdSe nanorods [59], we have to consider the anisotropy of the dipole matrix elements $|d_{\parallel}^a|^2$ and $|d_{\perp}^a|^2$. The anisotropy of the dipole matrix element can be taken into account, as previously, by replacing R in Eq. (18) with $r_a = Rf_a = R|d_{\parallel}^a|^2/|d_{\perp}^a|^2$. For example, the resonance excitation of the respective $F = \pm 1$ and $F = 0$ states is highly anisotropic and can be described by $r_a = f_a = 0$ and $r_a = f_a = \infty$, for any value of the local field effect anisotropy R . From the modified Eq. (18) for the $F = \pm 1$ exciton resonance absorption, we obtain the anisotropy degrees $\rho_{\pm 1}(\Theta, 0) = -\sin^2 \Theta / (1 + \cos^2 \Theta)$, which is equal to -0.5 at $\Theta = 90^\circ$. For the resonance absorption by $F = 0$ excitons, we obtain $\rho_0(\Theta, 0) = 1$.

The dot-in-rod (DiR) CdSe colloidal structures have demonstrated a higher photoluminescence quantum yield than CdSe nanorods and were suggested as polarized single-photon sources [60]. A 75% polarization was reported in a single CdSe/CdS core/shell DiR at room temperature [60]. Interestingly, while the anisotropy parameter $R > 1$ of the local field effect in these structures is completely determined by the shape of the CdS rod shell, the exciton fine structure is determined by the radius and shape of the CdSe core (whose c axis is directed along the long axis of the rod) as well as by the thickness of the CdS shell [61, 62]. It was shown, for example, that as the diameter of the CdSe core increases, the photoluminescence polarization in these structures changes from the one typical for sphere-like CdSe NCs to that typical for rod-like structures [62]. These transformations, in principle, can be described using the exciton selection-rule parameter f_d even at room temperature. However, PL linearly polarized along the c axis [61, 62] or at some

angle to the c axis [63] has been reported for different CdSe/CdS DiR structures at room temperatures. In contrast, the room-temperature emission of single spherical CdSe NCs and CdSe/CdS core/shell structures was reported to demonstrate properties of a degenerate 2D dipole at room [64, 65] as well as low [66] temperatures. Clearly, the room-temperature linear polarization of CdSe/CdS DiR nanostructures is primarily determined by the anisotropy of the local field effect, dictating $r_d > 1$. But the polarization properties of the CdSe/CdS DiR structures having a sphere-like band-edge exciton symmetry may change as the temperature decreases due to the decrease in the exciton anisotropy parameter $f_d < 1$, resulting in $r_d < 1$.

5. POLARIZATION MEMORY EFFECT

The angle-dependent probability P_e of optical transitions was first taken into account to describe the polarization properties of luminescence in porous Si [7, 53]. The porous Si was considered as an aggregate of dielectric ellipsoids embedded in an effective dielectric medium. In the case of random orientation of the ellipsoids, averaging P_e over all orientations cancels any polarization of absorption. But in the case of an excitation with linearly polarized light, the intensity of light emitted from an individual particle is given by $I_{PL}(\mathbf{e}_a, \mathbf{e}_d) \propto P_{e_a}(\omega_a)P_{e_d}(\omega_d)$, where \mathbf{e}_a and \mathbf{e}_d are the polarization vectors of the absorbed and emitted light. Averaging I_{PL} over the random orientations of the NC c -axis with respect to the light wave vector \mathbf{k} results in a nonzero degree of polarization memory,

$$P_{mem} = \frac{I_{\parallel} - I_{\perp}}{I_{\parallel} + I_{\perp}} = \frac{(R - 1)^2}{7 + 6R + 2R^2}, \quad (26)$$

where $I_{\parallel} = \langle I_{PL}(\mathbf{e}_a, \mathbf{e}_d \parallel \mathbf{e}_a) \rangle$ and $I_{\perp} = \langle I_{PL}(\mathbf{e}_a, \mathbf{e}_d \perp \mathbf{e}_a) \rangle$. We assume in Eq. (26) that PL is collected along the direction of the sample excitation and that the anisotropy parameter $R = D_{\parallel}/D_{\perp}$ is the same for absorbed and detected light. The anisotropy of the exciton selection rules is not included in Eq. (26).

In addition, the anisotropy of this polarization memory effect (the dependence of P_{mem} on the polarization \mathbf{e}_a) was experimentally observed for porous Si and explained by taking the distribution of ellipsoidal shapes and their orientation in the ensemble into account [7]. The effect of the NC alignment can be taken into account by introducing an NC distribution function $f_{align}(\Theta, \Phi)$ into the expressions for I_{\parallel} and I_{\perp} before the angular averaging procedure. Analysis of the experimental data allowed determining the ratio of the

effective volumes of elongated to flattened ellipsoids as approximately 9 to 1 and concluding that the long axes of the elongated ellipsoids are predominantly oriented along the [100] direction, whereas those of the flattened ellipsoids are predominantly perpendicular to this direction [7]. Further investigations with the pump-probe technique allowed observing the effect of optically induced anisotropy in porous Si based on selective excitations by a polarized pump beam together with the complete suppression of photoluminescence by nonradiative Auger processes in crystals with an additional hole and/or electron [8, 25].

In considering the polarization memory effect in an ensemble of colloidal NSs, it is important, as previously, to take the polarization anisotropy of the emitting ($r_d = Rf_d = R|d_{\parallel}^d|^2/|d_{\perp}^d|^2$) and absorbing ($r_a = Rf_a = R|d_{\parallel}^a|^2/|d_{\perp}^a|^2$) exciton states into account. Such a generalization results in the degree of linear polarization memory

$$P_{mem} = \frac{(r_a - 1)(r_d - 1)}{7 + 3r_d + r_a(3 + 2r_d)}. \quad (27)$$

Equation (27) was obtained for an ensemble of randomly oriented NCs. However, the consideration can be extended to include the NC alignment described by f_{align} .

In the foregoing, we have discussed selection rules for dipole-allowed “bright” exciton optical states. But at cryogenic temperatures, the polarization properties of colloidal NSs are determined by the lowest exciton state, which is known to be the spin-forbidden “dark” exciton. In the most commonly studied spherical or slightly deformed CdSe NCs, the lowest exciton state is the dark exciton state with the momentum projection $F = \pm 2$ on the c axis [23]. Recent magnetic field measurements [24, 67] indicate that the state with the momentum projection $F = \pm 2$ on the hexagonal c -axis is the lowest exciton state also in the CdSe/CdS DiR NSs. Dark-exciton recombination is forbidden in the dipole approximation unless the bright exciton states with the momentum projection $F = \pm 1$ or $F = 0$ are admixed to it by some perturbations [24, 68, 69]. The dipole-moment matrix elements $|d_{\perp}^{\pm 2}|^2$ and $|d_{\parallel}^{\pm 2}|^2$ acquired by the $F = \pm 2$ excitons due to the admixture of the respective $F = \pm 1$ and $F = 0$ exciton states are then determined by the admixture mechanisms [69].

Even without exact knowledge of the dark-exciton activation mechanism to be discussed in Ref. [69], the introduction of the anisotropy parameter $r_d = Rf_d = R|d_{\parallel}^{\pm 2}|^2/|d_{\perp}^{\pm 2}|^2$ allows analyzing the linear polarization properties and the degree of circular polarization induced by an external magnetic field of a single NS and

ensembles of these randomly oriented NSs [24]. For an individual NS, the degree of linear polarization ρ of the emitted light is given again by Eq. (18) with R replaced by r_d . The f_d parameter for the dark exciton may also depend on the external magnetic field due to the field-induced admixture of the $F = \pm 1$ exciton states [23]. This would result in a magnetic field dependence of ρ [24]. For the analysis of the polarization memory effect in the case of a dark exciton emitting state, Eq. (27) can be directly applied in a zero magnetic field. To consider the dark-exciton polarization in an external magnetic field, we have to take the dependence of f_d on the angle between the direction of magnetic field and the c axis into account in the averaging procedure (see Eq. (16) in Ref. [24]). In what follows, we consider the linear polarization memory effect only in a zero magnetic field.

The linear polarization memory effect with $P_{mem} \neq 0$ can be observed only when both emitting and absorption properties are anisotropic either due to the anisotropy of the exciton states with $|d_{\parallel}|^2 \neq |d_{\perp}|^2$ or due to the anisotropy of the local field effect $R \neq 1$. As discussed above, the anisotropy of absorption can be realized via resonance excitation of the $F = \pm 1$ state, resulting in $r_a = 0$, or the resonance excitation of the $F = 0$ state, resulting in $r_a = \infty$. For these two resonance excitation scenarios, Eq. (27) gives the following degree of memory polarization $P_{mem}^{(1)}$ and $P_{mem}^{(0)}$:

$$P_{mem}^{(1)} = \frac{1 - r_d}{7 + 3r_d}, \quad P_{mem}^{(0)} = \frac{r_d - 1}{3 + 2r_d}. \quad (28)$$

Thus, measuring the degree of linear polarization memory effect P_{mem} in resonant and nonresonant excitation conditions allows obtaining information on the exciton energy fine structure, on the origin of exciton-emitting states, and on the dark-exciton activation mechanisms at low temperatures in nanostructures with a known local field anisotropy parameter R .

Figure 5 shows the dependences of the degree of polarization memory effect P_{mem} under the nonresonant excitation ($f_a = 1$) of a randomly oriented ensemble on $1/R = D_x/D_z$ for prolate NCs with $b/c \leq 1$ and on $R = D_z/D_x$ for oblate NCs with $c/b \leq 1$. We can see that the largest degree of positive and negative polarization memory is reached in prolate NCs. In the case of isotropic selection rules for the emitting exciton (the grey line for $f_d = 1$), the polarization memory effect is always positive and can be observed only in the case of strong local field anisotropy: $1/R < 0.5$ in prolate or $R < 0.5$ in oblate NCs. In prolate NCs, the negative polarization memory can be observed for an anisotropic emission state with $f_d < 0.1$. In the limit $1/R \rightarrow 0$,

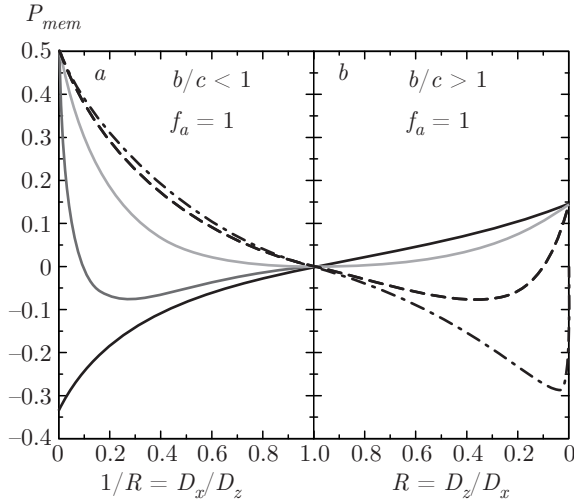


Fig. 5. Dependences of the polarization memory degree P_{mem} from a randomly oriented ensemble (a) on $1/R = D_x/D_z$ for prolate NSs with $b/c \leq 1$ and (b) on $R = D_z/D_x$ for oblate NSs with $b/c \geq 1$. Calculations are conducted for ellipsoidal-shape NSs excited in the isotropic absorbing exciton state with $f_a = 1$. The polarization properties of the emitting states are described as $f_d = 0$ (thick solid lines), $f_d = 0$ (thin solid lines), $f_d = 1$ (grey lines), $f_d = 10$ (dashed lines), and $f_d = 1000$ (dot-dashed lines)

we always have $P_{mem} \rightarrow 0.5$, except in the limit case where $f_d = 0$. In prolate NCs, negative polarization memory can be observed for anisotropic emission with $f_d > 10$. In spherical NCs with $R = 1$, the polarization memory effect cannot be observed for nonresonant excitation. But in NCs with a very small deviations of R from unity, the polarization memory effect can vary from -0.1 to 0.05 due to the anisotropy of the exciton-emitting state $f_d \neq 1$.

By contrast, the resonant excitation of NCs with $f_a \neq 1$ allows observing the polarization memory effect even in spherical NCs. Figure 6 shows the dependences of the polarization memory degree $P_{mem} = P_{mem}^{(1)}$ under the resonant excitation ($f_a = 0$) in a randomly oriented ensemble on $1/R = D_x/D_z$ for prolate NCs with $b/c \leq 1$ and on $R = D_z/D_x$ for oblate NCs with $c/b \leq 1$. We can see that in this case of the resonance excitation of a transverse exciton $f_a = 0$, the maximum polarization memory degree is $1/7$. This $1/7$ polarization can be observed if the emitting state has the same symmetry $f_d = 0$ as the exciting state. In contrast, in the exciton-emitting state polarized along the c axis, the polarization memory effect is always negative and reaches the maximum negative value $-1/3$. In spherical NCs with $R \approx 1$, the positive and negative values of the polarization memory indicate the respective anisotropy

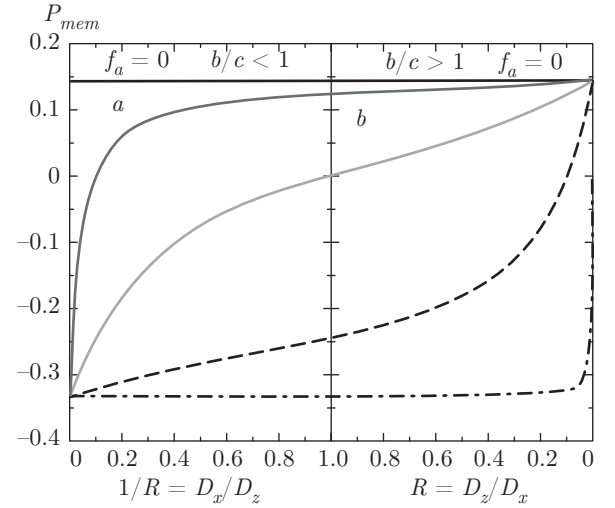


Fig. 6. Dependences of the polarization memory degree P_{mem} from a randomly oriented ensemble (a) on $1/R = D_x/D_z$ for prolate NSs with $b/c \leq 1$ and (b) on $R = D_z/D_x$ for oblate NSs with $b/c \geq 1$. Calculations are conducted for ellipsoidal-shape NSs that are excited in the transverse absorbing exciton state with $f_a = 0$. The polarization properties of the emitting states are described as $f_d = 0$ (thick solid lines), $f_d = 0$ (thin solid lines), $f_d = 1$ (grey lines), $f_d = 10$ (dashed lines), and $f_d = 1000$ (dot-dashed lines)

of the exciton emitting state $f_d < 1$ and $f_d > 1$.

The positive and negative polarization memory degrees were reported in Ref. [70] for time-resolved PL measurements under the resonant excitation of the $F = \pm 1$ exciton state in spherical CdSe NCs. The positive value $P_{mem}^{(1)} = 1/7$ for $r_d = 0$ excellently describes the polarization of emission from the same bright-exciton $F = \pm 1$ state just after its excitation¹⁾ [70]. The negative polarization memory $P_{mem}^{(1)} \approx -0.14$ was observed at a temperature of about 10 K after the relaxation of the exciton to the lowest dark-exciton state. Equation (28) allows extracting the anisotropic parameter as $r_d = (1 - 7P_{mem}^{(1)})/(1 + 3P_{mem}^{(1)}) \approx 3.41$. As the local field parameter R for the spherical NCs approaches unity, we can estimate the polarization anisotropy of dark-exciton recombination $f_d \approx 3.41$ in the studied CdSe NCs at $T = 10$ K. In this particular situation, the dark exciton seems to inherit the properties of the 1D dipole from the $F = 0$ bright-exciton state rather than the 2D dipole properties from the $F = \pm 1$ excitons. As was shown in Ref. [68], the effective mechanism of dark-exciton recombination in CdSe

¹⁾ In the Ref. [70], the value $\rho = (I_{\parallel} - I_{\perp})/(I_{\parallel} + 2I_{\perp})$ was reported which can be converted into the degree of linear polarization memory as $P_{mem} = 3\rho/(\rho + 2)$.

NCs is the surface dangling-bond spin-flip-assisted recombination, which has the polarization properties of a 2D dipole. However, this mechanism can be suppressed at low temperatures in small-size NCs due to the dynamic polarization of the dangling-bond spins and the formation of a dangling-bond magnetic polaron [68]. Indeed, the observed negative polarization memory nearly vanishes with an increase in temperature above 20 K [70].

Generally, the emission anisotropy polarization parameter f_d (and hence r_d) may depend on the temperature (see, e.g., Eq. (25)), time (in time-resolved experiments due to the exciton relaxation after excitation), and external magnetic field [24]. Importantly, the same parameters r_d and r_a control the degree of circular polarization in an external magnetic field [24]. For example, analysis of the degree of circular polarization in CdSe/CdS DiR NSs with different aspect ratios b/c and therefore different local field parameters $R \geq 1$ allowed estimating the values of r_d as $0 \leq r_d \leq 1$ and therefore $0 \leq f_d \leq 1$ for all investigated samples at low temperatures [24]. In the investigated DiR structures, the dark exciton inherited the properties of a 2D dipole polarized perpendicular to the c axis. A further insight into the exciton fine energy structure in DiR structures and exciton anisotropy can be obtained from temperature-dependent and time-resolved measurements of the polarization memory effect.

6. SUMMARY

To summarize, we have discussed the effects caused by strong dielectric confinement on the optical properties of NSs with different shapes, e.g., NCs, nanorods and nanoplatelets. In spherical NCs, the most important phenomenon is the reduction of the exciton radiative decay rate due to the local field effect. In 1D and 2D colloidal NSs, the coupling of excitons to photons is not reduced for an electric field polarized along the long axis, while the exciton oscillator strength is enhanced. As a result, we should expect an increase in the radiative decay rate. The polarization properties of an ensemble of randomly oriented colloidal NCs are controlled by both the anisotropy of the local field effect and by the symmetry of the exciton states. We have shown that measuring the linear polarization memory effect at low temperatures can reveal the exciton fine structure and the activation mechanisms of the lowest dark exciton responsible for its radiative decay.

The authors thank S. G. Tikhodeev, M. Johannes, and E. A. Zhukov for help and the stimulating discussions. The work of A. V. R was supported by

the RFBR (Grant No.13-02-00888) and by the Government of Russia (Project No.14.Z50.31.0021, leading scientist M. Bayer). Al. L. E. acknowledges the financial support of the Office of Naval Research (ONR) through the Naval Research Laboratory Basic Research Program.

REFERENCES

1. L. V. Keldysh, Pis'ma v Zh. Eksp. Teor. Fiz. **29**, 716 (1979) [JETP Lett. **29**, 658 (1979)].
2. N. S. Rytova, Vestn. Mosk. Univ. **3**, 30 (1967).
3. V. S. Babichenko, L. V. Keldysh, and A. P. Silin, Fiz. Tverd. Tela **22**, 1238 (1980) [Sov. Phys. Solid State **22**, 723 (1980)].
4. L. V. Keldysh, Superlatt. and Microstruct. **4**, 637 (1988).
5. L. V. Keldysh, Phys. Stat. Sol. (a) **164**, 3 (1997).
6. N. A. Gippius, S. G. Tikhodeev, V. D. Kulakovskii, and A. Forchel, Pis'ma v Zh. Eksp. Teor. Fiz. **59**, 527 (1994) [JETP Lett. **59**, 556 (1994)].
7. D. Kovalev, M. Ben Chorin, J. Diener et al., Appl. Phys. Lett. **67**, 1585 (1995).
8. D. Kovalev, B. Averboukh, M. Ben Chorin et al., Phys. Rev. Lett. **77**, 2089 (1996).
9. S. A. Gavrilov, V. V. Gusev, V. S. Dneprovskii et al., Pis'ma v Zh. Eksp. Teor. Fiz. **70**, 216 (1999) [JETP Lett. **70**, 216 (1999)].
10. E. A. Muljarov, E. A. Zhukov, V. S. Dneprovskii, and Y. Masumoto, Phys. Rev. B **62**, 7420 (2000).
11. A. Shabaev and Al. L. Efros, Nano Lett. **4**, 1821 (2004).
12. A. C. Bartnik, Al. L. Efros, W.-K. Koh, C. B. Murray, and F. W. Wise, Phys. Rev. B **82**, 195313 (2010).
13. J. S. Kamal, R. Gomes, Z. Hens et al., Phys. Rev. B **85**, 035126 (2012).
14. R. Benchamekh, N. A. Gippius, J. Even et al., Phys. Rev. B **89**, 035307 (2014).
15. A. W. Achtstein, A. Schliwa, A. Prudnikau et al., Nano Lett. **12**, 3151 (2012).
16. S. Schmitt-Rink, D. A. B. Miller, and D. S. Chemla, Phys. Rev. B **35**, 8113 (1987).
17. E. Yablonovitch, T. G. Gmitter, and R. Bhat, Phys. Rev. Lett. **61**, 2546 (1988).

18. L. D. Landau and E. M. Lifshitz, *Electrodynamics of Continuous Media*, Pergamon Press, Oxford (1960).
19. N. A. Gippius, E. A. Muljarov, J. Rubio et al., *Phys. Stat. Sol. (b)* **188**, 269 (1995).
20. P. Ils, Ch. Greus, A. Forchel et al., *Phys. Rev. B* **51**, 4272 (1995).
21. Al. L. Efros, *Phys. Rev. B* **46**, 7448 (1992).
22. M. Chamarro, C. Gourdon, P. Lavallard, O. Lublinskaya, and A. I. Ekimov, *Phys. Rev. B* **53**, 1336 (1996).
23. Al. L. Efros, in: *Semiconductor and Metal Nanocrystals: Synthesis and Electronic and Optical Properties*, ed. by V. I. Klimov, Marcel Dekker, New York (2003), Chap. 3, p. 103.
24. B. Siebers, L. Biadala, D. R. Yakovlev et al., *Phys. Rev. B* **91**, 155304 (2015).
25. Al. L. Efros, M. Rosen, B. Averboukh et al., *Phys. Rev. B* **56**, 3875 (1997).
26. L. V. Kulik, V. D. Kulakovskii, M. Bayer et al., *Phys. Rev. B* **54**, R2335 (1996).
27. N. A. Gippius, A. L. Yablonskii, A. B. Dzyubenko et al., *J. Appl. Phys.* **83**, 5410 (1998).
28. E. A. Muljarov, S. G. Tikhodeev, N. A. Gippius, and T. Ishihara, *Phys. Rev. B* **51**, 14370 (1995).
29. L. E. Brus, *J. Chem. Phys.* **79**, 5566 (1983).
30. L. E. Brus, *J. Chem. Phys.* **80**, 4404 (1984).
31. T. Takagahara, *Phys. Rev. B* **39**, 10206 (1989).
32. G. B. Grigoryan, A. V. Rodina, and Al. L. Efros, *Fiz. Tverd. Tela* **32**, 3512 (1990) [*Sov. Phys. Sol. State* **32**, 2037 (1990)].
33. T. Takagahara, *Phys. Rev. B* **47**, 4569 (1993).
34. J. D. Jackson, *Classical Electrodynamics*, 3rd ed., Wiley, New York (1998).
35. V. V. Batygin and I. N. Toptygin, *Sbornik Zadach po Elektrodinamike*, 3rd ed., Nauka, Moscow (1970).
36. L. Banyai, P. Gilliot, Y. Z. Hu, and S. W. Koch, *Phys. Rev. B* **45**, 14136 (1992).
37. Y. M. Niquet, C. Delerue, G. Allan, and M. Lannoo, *Phys. Rev. B* **65**, 165334 (2002).
38. L. Jdira, P. Liljeroth, E. Stoffels, D. Vanmaekelbergh, and S. Speller, *Phys. Rev. B* **73**, 115305 (2006).
39. K. A. Svit and K. S. Zhuravlev, *J. Phys. Chem. C* **119**, 19496 (2015).
40. S. Ithurria, M. D. Tessier, M. P. S. M. Lobo, B. Dubertret, and Al. L. Efros, *Nat. Mater.* **10**, 936 (2011).
41. J. Even, L. Pedesseau, and M. Kepenekian, *Phys. Chem. Chem. Phys.* **16**, 25182 (2014).
42. L. Biadala, F. Liu, M. D. Tessier et al., *Nano Lett.* **14**, 1134 (2014).
43. M. Olutas, B. Guzelturk, Y. Kelestemur et al., *ACS Nano* **9**, 5041 (2015).
44. C. Delerue, M. Lannoo, and G. Allan, *Phys. Rev. B* **68**, 115411 (2003).
45. A. D. Yoffe, *Adv. Phys.* **42**, 173 (1993).
46. H. Haken, *Z. Phys.* **146**, 527 (1957).
47. J. Pollmann and H. Buettner, *Phys. Rev. B* **16**, 4480 (1977).
48. S. V. Goupalov, *Phys. Rev. B* **68**, 125311 (2003).
49. A. N. Poddubny, *J. Optics* **17**, 035102 (2015).
50. K. K. Pukhov, T. T. Basiev, and Y. V. Orlovskii, *Pis'ma v Zh. Eksp. Teor. Fiz.* **88**, 14 (2008) [*JETP Lett.* **88**, 12 (2008)].
51. V. S. Dneprovskii, E. A. Zhukov, O. A. Shalygina et al., *Zh. Eksp. Teor. Fiz.* **121**, 1362 (2002) [*JETP* **94**, 1169 (2002)].
52. J. Wang, M. S. Gudiksen, X. Duan, Yi Cui, and Ch. M. Lieber, *Science* **293**, 1455 (2001).
53. P. Lavallard and R. A. Suris, *Sol. St. Comm.* **95**, 267 (1995).
54. Al. L. Efros and W. R. L. Lambrecht, *Phys. Rev. B* **89**, 035304 (2014).
55. D. Spirkoska, Al. L. Efros, W. R. L. Lambrecht et al., *Phys. Rev. B* **85**, 045309 (2012).
56. N. Le Thomas, E. Herz, O. Schöps, U. Woggon, and M. V. Artemyev, *Phys. Rev. Lett.* **94**, 016803 (2005).
57. J. T. Hu, L. S. Li, W. D. Yang et al., *Science* **292**, 2060 (2001).
58. S. A. Crooker, T. Barrick, J. A. Hollingsworth, and V. I. Klimov, *Appl. Phys. Lett.* **82**, 2793 (2003).
59. D. B. Tice, D. J. Weinberg, N. Mathew, R. P. H. Chang, and E. A. Weiss, *J. Phys. Chem. C* **117**, 13289 (2013).
60. F. Pisanello, L. Martiradonna, P. Spinicelli et al., *Superlattices and Microstructures* **47**, 165 (2010).
61. B. T. Diroll, A. Koschitzky, and Ch. B. Murray, *J. Phys. Chem. Lett.* **5**, 85 (2014).

62. S. Vezzoli, M. Manceau, G. Lemenager et al., *ACS Nano* **9**, 7992 (2015).
63. C. Lethiec, F. Pisanello, L. Carbone, A. Bramati, L. Coolen, and A. Maitre, *New J. Physics* **16**, 093014 (2014).
64. C. Lethiec, J. Laverdant, H. Vallon et al., *Phys. Rev. X* **4**, 021037 (2014).
65. I. Chung, K. T. Shimizu, and M. G. Bawendi, *Proc. Natl. Acad. Sci. U.S.A.* **100**, 405 (2003).
66. S. A. Empedocles, R. Neuhauser, and M. G. Bawendi, *Nature* **399**, 126 (1999).
67. A. G. del Aguila, B. Jha, F. Pietra et al., *ACS Nano* **8**, 5921 (2014).
68. A. Rodina and Al. L. Efros, *Nano Lett.* **15**, 4214 (2015).
69. A. Rodina and Al. L. Efros, Private communication.
70. M. G. Bawendi, P. J. Carroll, W. L. Wilson, and L. E. Brus, *J. Chem. Phys.* **96**, 946 (1992).